Journal of Computational Physics 302 (2015) 420–438

Contents lists available at ScienceDirect

Journal of Computational Physics

www.elsevier.com/locate/jcp

An adhesive contact mechanics formulation based on atomistically induced surface traction

Houfu Fan [a], Bo Ren [b], Shaofan Li [a,*]

[a] Department of Civil and Environmental Engineering, University of California, Berkeley, CA 94720, United States
[b] Livermore Software Technology Corporation, 7374 Las Positas Road, Livermore, CA 94551, United States

ARTICLE INFO

Article history:
Received 24 December 2014
Received in revised form 8 August 2015
Accepted 19 August 2015
Available online 14 September 2015

Keywords:
Adhesive contact
Derjuguin approximation
Finite element
Multiscale simulation
Surface traction

ABSTRACT

In this work, we have developed a novel multiscale computational contact formulation based on the generalized Derjuguin approximation for continua that are characterized by atomistically enriched constitutive relations in order to study macroscopic interaction between arbitrarily shaped deformable continua. The proposed adhesive contact formulation makes use of the microscopic interaction forces between individual particles in the interacting bodies. In particular, the double-layer volume integral describing the contact interaction (energy, force vector, matrix) is converted into a double-layer surface integral through a mathematically consistent approach that employs the divergence theorem and a special partitioning technique. The proposed contact model is formulated in the nonlinear continuum mechanics framework and implemented using the standard finite element method. With no large penalty constant, the stiffness matrix of the system will in general be well-conditioned, which is of great significance for quasi-static analysis. Three numerical examples are presented to illustrate the capability of the proposed method. Results indicate that with the same mesh configuration, the finite element computation based on the surface integral approach is faster and more accurate than the volume integral based approach. In addition, the proposed approach is energy preserving even in a very long dynamic simulation.

1. Introduction

Contact that occurs at the interface between different continuum objects transmits forces. Classical (Hertz) contact between deformable bodies under large deformations has been extensively studied in computational contact mechanics, all of which are mainly focused on contact between large-scale objects governed by the principles of continuum mechanics and the no-penetrability condition [1,2]. With the increasing demand in nano-engineering and nano-science, the treatment of adhesive contact at nano/micro scale is becoming more and more important. The applications of small scale contact interaction range from nanoindentation [3–5], flexible nanotubes [6,7], MEMS design [8], atomic force microscopy [9–11], DNA strands and proteins [12], dynamic droplet spreading [13,14], to the contact/adhesion/crawling of living cells [15,16].

The adhesive contact phenomena at small scale can be modeled by several theoretical models, such as Johnson, Kendall and Roberts (JKR) model [17] and Derjaguin, Muller and Toporov (DMT) model [18]. Finite element based numerical methods have also be employed in modeling the adhesive/contact [19]. These analytical or numerical models have been successfully

* Corresponding author. Tel.: +1 (510) 642 5362; fax: +1 (510) 643 8928.
E-mail address: shaofan@berkeley.edu (S. Li).

http://dx.doi.org/10.1016/j.jcp.2015.08.035
0021-9991/

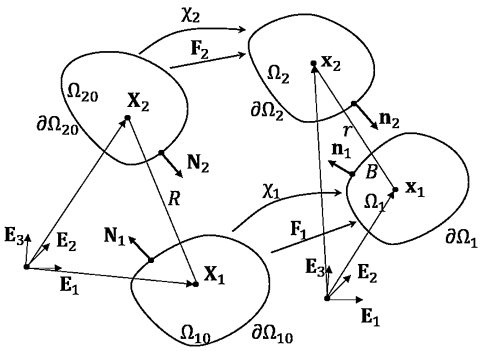

Fig. 1. Continuum description of the contact model.

applied to a lot of areas, but they have their intrinsic limitations, by either assuming infinitesimal deformations, contacting bodies with special geometries, or requiring one of the contacting body to be rigid, which substantially simplifies the computational treatment. Microscopically, the contact interaction of two bodies originates from the inter-body interaction of individual atoms or molecules. In principle, one can always directly simulate the problem using molecular dynamics [20–22], which essentially treats all participating atoms as classical objects whose motions are governed by the Newton's second law. But due to the intrinsic limitations [20], most of the studies using molecular dynamics mainly focus on the general principles, instead of practical applications in nano-engineering.

An appropriate model for describing such small scale contact/adhesion, should incorporate the microscopic interactions of the underlying atoms/molecules, formulate in nonlinear continuum mechanics framework, and at the same time maintain low computation cost. Similarly to classic Barrier contact method [1,23], one can characterize the small scale contact by introducing the inter-body interaction potentials between atoms/molecules into the total potential energy of the system. One of the advantages of this method is that it does not require any large penalty constant, such that the contact stiffness matrix of the system is in general well-conditioned. However, if one directly applies the body to body atomistic interaction potential to the system, the computational cost would be so large that no practical engineering problem can be solved. In this work, the double-layer volume integral describing the contact interaction (energy, force vector, matrix) is converted into a double-layer surface integral through a mathematically consistent approach that employs the divergence theorem and a special partitioning technique. Based on resulting surface formulation, a novel multiscale computational contact model is developed. We want to mention that the contact model developed here works for problems in both two and three dimensional space. A similar approach is accomplished in [24,25] for two-dimensional problem with certain physical assumptions.

The proposed contact model is formulated in the framework of nonlinear continuum mechanics and implemented for both quasi-static and explicit dynamic analysis. Results show that with the same mesh configuration, the proposed surface integral approach is faster and more accurate than the one directly applies the volume integral. The dynamic simulation of impact of the two cylinders within a rigid frame reveals that the proposed model is energy preserving in a long time dynamic simulation.

The paper is organized into five sections. In Section 2, the problem description of the multiscale contact model is presented in the framework of nonlinear continuum mechanics. In Section 3, the conversion from the double-layer volume integral to a double-layer surface integral for the contact model is presented. Section 4 deals with the Galerkin weak formulation of the proposed contact model. In Section 5, the details of finite element implementation for both quasi-static and dynamic cases of the multiscale contact model are being discussed. In Section 6, several numerical examples are presented with some discussions are provided. Finally in Section 7, we close the presentation by making a few remarks.

2. Problem description

We are considering two interacting bodies 1 and 2, as shown in Fig. 1. Subjected to certain boundary conditions (not shown in the figure) and the inter-body contact interactions, the two bodies originally occupying the physical domains Ω_{10}, Ω_{20} deform and evolve to Ω_1, Ω_2 in the current configuration. Correspondingly, the boundaries (surfaces) and unit out-normals of the two bodies change from $\partial\Omega_{10}$, $\partial\Omega_{20}$ and $\mathbf{N}_1$, $\mathbf{N}_2$ to $\partial\Omega_1$, $\partial\Omega_2$ and $\mathbf{n}_1$, $\mathbf{n}_2$.

If the system is conservative, the total potential energy of the system can be written as,

$$\Pi^{total} = \sum_{I=1}^{2} \left(\Pi^{int,I} + \Pi^{ext,I} \right) + \Pi^{C}, \tag{1}$$

where $\Pi^{int,I}$ is the internal elastic energy, $\Pi^{ext,I}$ is the external potential energy and Π^{C} represents the interaction potential energy due to the adhesive contact. In general, the internal elastic energy

$$\Pi^{int,I} = \int_{\Omega_{I0}} W(\mathbf{F}_I) dV_I \tag{2}$$

and external potential energy

$$\Pi^{ext,I} = -\int_{\Omega_I} \rho_I \mathbf{b}_I \cdot \mathbf{u}_I dv_I - \int_{\partial\Omega_{IT}} \mathbf{t}_I \cdot \mathbf{u}_I ds \tag{3}$$

where $I = 1, 2$ denotes the two interacting bodies. $\mathbf{F}_I$ is the deformation gradient tensor, $W(\mathbf{F}_I)$ the energy per unit reference volume, $\mathbf{u}_I$ the displacement field, $\mathbf{b}_I$ the body force and $\mathbf{t}_I$ the traction force on the Neumann boundary $\partial\Omega_{IT}$.

From microscopic perspective, the internal energy $\Pi^{int,I}$ can be viewed as the potential characterizing the short range particle interactions within body I, which is mainly due to the covalent or ionic bonds. On the other hand, Π^C comes from the interactions between atoms/molecules from two different bodies, which could originate from different physical phenomena [26]. Normally it can be described by a potential energy that is dependent on their relative position. Generally only long range forces prevail in terms of the interaction between two adjacent bodies. Thus the long range van der Waals interaction is a suitable candidate for describing the inter-body interactions. In this work, the inter-body particle interaction is modeled by the 12–6 Lennard Jones potential

$$\phi(r) = \varepsilon \left[\left(\frac{\sigma_0}{r}\right)^{12} - 2\left(\frac{\sigma_0}{r}\right)^{6} \right], \tag{4}$$

where ε is the depth of the potential well (in the unit of energy) and σ_0 is the equilibrium distance. The r^{-12} term characterizes the short range Pauli repulsion force resulting from electron orbital overlapping, preventing the two particles being much too close. Summing up all the inter-body interactions between particles in the two bodies, one may arrive at the final form of the homogenized interaction energy for the adhesive contact,

$$\Pi^C = \int_{\Omega_1}\int_{\Omega_2} \beta_1\beta_2\phi(r) dv_2 dv_1, r = |\mathbf{x}_1 - \mathbf{x}_2|, \tag{5}$$

where β_1 and β_2 represent the current particle densities located at points $\mathbf{x}_1 \in \Omega_1$ and $\mathbf{x}_2 \in \Omega_2$.

The first variation of the contact interaction energy is,

$$\delta\Pi^C = \int_{\Omega_1}\int_{\Omega_2} \beta_1\beta_2 \left(\frac{\partial\phi(r)}{\partial\mathbf{x}_1} \cdot \delta\mathbf{u}_1 + \frac{\partial\phi(r)}{\partial\mathbf{x}_2} \cdot \delta\mathbf{u}_2 \right) dv_2 dv_1 \tag{6}$$

If we define

$$\bar{\mathbf{b}}_1(\mathbf{x}_1) := -\frac{\partial\Phi_2}{\partial\mathbf{x}_1}, \quad \Phi_2 = \int_{\Omega_2} \beta_2\phi(r) dv_2 \tag{7}$$

$$\bar{\mathbf{b}}_2(\mathbf{x}_2) := -\frac{\partial\Phi_1}{\partial\mathbf{x}_2}, \quad \Phi_1 = \int_{\Omega_1} \beta_1\phi(r) dv_1 \tag{8}$$

then

$$\delta\Pi^C = -\int_{\Omega_1} \beta_1\bar{\mathbf{b}}_1 \cdot \delta\mathbf{u}_1 - \int_{\Omega_2} \beta_2\bar{\mathbf{b}}_2 \cdot \delta\mathbf{u}_2 dv_2 \tag{9}$$

where $\bar{\mathbf{b}}_1$ and $\bar{\mathbf{b}}_2$ can be viewed as the body forces resulting from the adhesive contact.

Therefore the equilibrium equations of the multiscale contact problem can be expressed as

$$\begin{cases} \frac{\partial\boldsymbol{\sigma}_I}{\partial\mathbf{x}_I} + \mathbf{b}_I + \bar{\mathbf{b}}_I = \mathbf{0}, & \text{in} \quad \Omega_I \\ \mathbf{u}_I = \bar{\mathbf{u}}_{I0}, & \text{on} \quad \partial\Omega_{Iu} \\ \mathbf{t}_I = \boldsymbol{\sigma}_I\mathbf{n}_I = \bar{\mathbf{t}}_{I0}, & \text{on} \quad \partial\Omega_{It} \end{cases} \tag{10}$$

where $\bar{\mathbf{u}}_{I0}$ is the fixed displacement on the essential boundary $\partial\Omega_{Iu}$ and $\bar{\mathbf{t}}_{I0}$ is the traction force on the boundary $\partial\Omega_{It}$.

Obviously, one can directly solve the problem using standard finite element method (FEM) [27,28]. But as one may notice, Eq. (9) involves a double-layer integral over the volumes of the two bodies that requires huge computational cost, posing great challenges if one wants to simulate a large system, especially in three-dimension space. In this work, we propose a different approach, such that the governing equations of the system can be expressed as

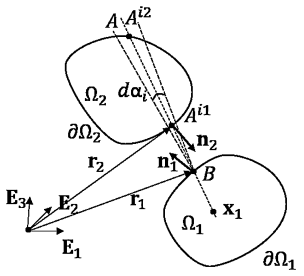

Fig. 2. The surface integral for the contact model.

$$\begin{cases} \frac{\partial \sigma_I}{\partial \mathbf{x}_I} + \mathbf{b}_I = \mathbf{0}, & \text{in} \quad \Omega_I \\ \mathbf{u}_I = \bar{\mathbf{u}}_{I0}, & \text{on} \quad \partial\Omega_{Iu} \\ \mathbf{t}_I = \boldsymbol{\sigma}_I^s \mathbf{n}_I + \bar{\mathbf{t}}_{I0}, & \text{on} \quad \partial\Omega_{It} \end{cases} \tag{11}$$

In addition to the usual applied traction forces $\bar{\mathbf{t}}_{I0}$, an extra traction forces $\mathbf{t}_I^s = \boldsymbol{\sigma}_I^s \mathbf{n}_I$, resulting from the contact interaction, is applied to the system. $\boldsymbol{\sigma}_I^s$ can be viewed as the surface stress tensors coming from the contact interaction. Details of the surface stress tensors will be shown in the next section.

3. Surface integral for the contact model

Following the approach outlined in [29,30], we convert the double-layer volume integral to a double-layer surface integral in context of continuum mechanics. As shown in Fig. 1, the force applying on an infinitesimal volume element dv_1 in body Ω_1 due to the presence of an infinitesimal volume element dv_2 can be written as,

$$d\mathbf{f} = -\beta_1\beta_2 \frac{\partial \phi(r)}{\partial \mathbf{x}_1} dv_1 dv_2 = \beta_1\beta_2 \frac{\partial \phi(r)}{\partial \mathbf{x}_2} dv_1 dv_2, \tag{12}$$

where $\mathbf{x}_1$ is the position vector of a generic particle in body Ω_1 with a volume dv_1 and $\mathbf{x}_2$ that of a generic particle in body Ω_2 with a volume dv_2. The relative distance is defined as $r := |\mathbf{x}_1 - \mathbf{x}_2|$. It is easy to see that the interaction force density in Ω_1 due to Ω_2 can be written as,

$$\hat{\mathbf{b}}_1 = \int_{\Omega_2} \frac{d\mathbf{f}}{dv_1} dv_2 = \int_{\Omega_2} \beta_1\beta_2 \frac{\partial \phi(r)}{\partial \mathbf{x}_2} dv_2 = \int_{\partial\Omega_2} \beta_1\beta_2\phi(r)\mathbf{n}_2 da_2, \tag{13}$$

where $\mathbf{n}_2$ and da_2 is the surface unit out normal and the corresponding area of the infinitesimal surface element at the point of interest on $\partial\Omega_2$, respectively. Thus the interaction force density in Ω_1 due to the presence of $da_2 \in \partial\Omega_2$ is

$$d\hat{\mathbf{b}}_1 = \beta_1\beta_2\phi(r)\mathbf{n}_2 da_2 \tag{14}$$

The corresponding interaction force in Ω_1 can then be expressed as

$$\mathbf{F}_1 = \int_{\Omega_1} d\hat{\mathbf{b}}_1 dv_1 = \beta_1\beta_2 \int_{\Omega_1} \phi(r)\mathbf{n}_2 da_2\, dv_1 \tag{15}$$

As shown in Fig. 2, if we partition Ω_1 into infinite number of spherical cones, with BA^{i1} the axis of these cones, then the infinitesimal volume element dv_1 can be expressed as $dv_1 = t^2 d\alpha dt$. B and A^{i1} are the intersection points on $\partial\Omega_2$ and $\partial\Omega_1$ when one connects the center of the volume element dv_1 with that of dv_2. $d\alpha_i$ is the solid angle of the cone, and t is the distance to the apex of the cone B. Notice that the force in Eq. (15) can be evaluated by the summation of a series of integrals along the cone axes,

$$\begin{aligned} \mathbf{F}_1 &= \beta_1\beta_2 \sum_{i=1}^{N_{cones}} (\mathbf{n}_2 da_2)\, d\alpha_i \int_{s_{i1}}^{s_{i2}} \phi(t) t^2 dt \\ &= \beta_1\beta_2 \sum_{i=1}^{N_{cones}} (\mathbf{n}_2 da_2)\, d\alpha_i \left(\int_{s_{i2}}^{\infty} \phi(t) t^2 dt - \int_{s_{i1}}^{\infty} \phi(t) t^2 dt \right) \end{aligned} \tag{16}$$

where s_{i1}, s_{i2} are distances from the apex of the i-th cone (B) to the intersections of the cone axis with $\partial\Omega_1$ (A^{i1} and A^{i2}), respectively.

It is assumed that the potential function $\phi(t)$ decays faster than $1/t^3$, such that the integrals in the equation above remain finite. Therefore the interaction force $\mathbf{F}_1$ in Ω_1 due to the presence of da_2 can now be written as the sum of a series of integrals,

$$\mathbf{F}_1 = \beta_1\beta_2 \sum_{i=1}^{N_{cones}} \left(\mathbf{n}_2 da_2 d\alpha_i \sum_{j=1}^{2} (-1)^{j+1} \int_{s_{ij}}^{\infty} \phi(t) t^2 dt \right) = \sum_{i=1}^{N_{cones}} \sum_{j=1}^{n_{int}} \mathbf{F}_1^{ij} = \sum_{k=1}^{N_{int}} d\mathbf{F}_1 \tag{17}$$

where N_{cones} represents the total number of infinitesimal spherical cones, n_{int} the number of intersections of the ith cone axis with $\partial\Omega_1$, N_{int} the total number of intersections with $\partial\Omega_1$ for all spherical cone axes, and $d\mathbf{F}_1 = \mathbf{F}_1^{ij}$ the contact interaction force corresponding to the jth intersection of the ith cone axis with $\partial\Omega_1$.

It is not hard to imagine that all together, these intersections points ($k = 1, N_{int}$) form exactly the surface $\partial\Omega_1$, if Ω_1 is discretized into infinite number of spherical cones such that the solid angle $d\alpha_i \to 0$, $i = 1, 2, \ldots$. The proposed partitioning of the interaction force $\mathbf{F}_1$ to $d\mathbf{F}_1$ aims to represent the successive contribution from each infinitesimal surface element da_1^i associated with a generic intersection point A^{ij} on $\partial\Omega_1$. The mathematical expression for $\mathbf{F}_1^{ij}$ is

$$\mathbf{F}_1^{ij} = \beta_1\beta_2 \mathbf{n}_2 da_2 d\alpha_i (-1)^{j+1} \int_{s_{ij}}^{\infty} \phi(t) t^2 \, dt \tag{18}$$

where s_{ij} is the distance from the apex B to the intersection A^{ij} and $d\alpha_j$ is the solid angle of the cone with axis BA^{ij}. Set $\mathbf{r}_1$ and $\mathbf{r}_2$ as the position vectors on $\partial\Omega_1$ and $\partial\Omega_2$, respectively, then direction of the cone axis can be obtained $\mathbf{e} = \mathbf{r}_{12}/s$, where $\mathbf{r}_{12} := \mathbf{r}_1 - \mathbf{r}_2$ and $s = \|\mathbf{r}_{12}\|$. Based on the definition of solid angle, $s_{ij}^2 d\alpha_j$ is the projection area of da_1^i onto the cone axis $\mathbf{e}$,

$$s_j^2 d\alpha_j = (-1)^{j+1} \mathbf{e} \cdot \mathbf{n}_1 da_1^i = (-1)^{j+1} \frac{1}{s_j} \mathbf{r}_{12} \cdot \mathbf{n}_1 da_1^i \tag{19}$$

where $\mathbf{n}_1$ is the unit surface out-normal at point $\mathbf{r}_1$. Substituting Eq. (19) into Eq. (18), one can obtain,

$$\mathbf{F}_1^{ij} = \beta_1\beta_2 (\mathbf{n}_2 \otimes \mathbf{r}_{12}) \cdot \mathbf{n}_1 da_2 da_1^i \frac{1}{s_{ij}^3} \int_{s_{ij}}^{\infty} \phi(t) t^2 dt \tag{20}$$

Define the function

$$\psi(r) = \frac{1}{r^3} \int_r^{\infty} \phi(t) t^2 \, dt, r > 0 \tag{21}$$

and drop the indices i and j, the force in Eq. (20) can be written as

$$d\mathbf{F}_1 = (\beta_1\beta_2 (\mathbf{n}_2 \otimes \mathbf{r}_{12}) \cdot \mathbf{n}_1 \psi(s)) \, da_2 da_1, \tag{22}$$

which represents the interaction force acting on an infinitesimal element $da_1 \in \partial\Omega_1$ due to the presence of $da_2 \in \partial\Omega_2$. Using the Nanson's formula $\mathbf{n}da = J\mathbf{F}^{-T}\mathbf{N}dA$, Eq. (22) can be rewritten as

$$d\mathbf{F}_1 = \left\{ \beta_{10}\beta_{20} \left[\left(\mathbf{F}^{-T}\mathbf{N}_2 \right) \otimes \mathbf{r}_{12} \right] \cdot \left(\mathbf{F}^{-T}\mathbf{N}_1 \right) \psi(s) \right\} dA_2 dA_1, \tag{23}$$

where β_{10}, β_{20} are the particle densities, $\mathbf{N}_1$, $\mathbf{N}_2$ the unit-out normals and dA_2, dA_1 the infinitesimal surface element areas in the reference configuration.

Similarly, the interaction force applied on an infinitesimal surface element $da_2 \in \partial\Omega_2$ due to the presence of an infinitesimal surface element $da_1 \in \partial\Omega_1$ can be derived as,

$$d\mathbf{F}_2 = (\beta_1\beta_2 (\mathbf{n}_1 \otimes \mathbf{r}_{21}) \cdot \mathbf{n}_2 \psi(s)) \, da_1 da_2, \tag{24}$$

Rewrite the equation above in the reference configuration, we have

$$d\mathbf{F}_2 = \left\{ \beta_{10}\beta_{20} \left[\left(\mathbf{F}^{-T}\mathbf{N}_1 \right) \otimes \mathbf{r}_{21} \right] \cdot \left(\mathbf{F}^{-T}\mathbf{N}_2 \right) \psi(s) \right\} dA_1 dA_2, \tag{25}$$

Reorganizing Eq. (22) and (24), one may get

$$\frac{d\mathbf{F}_1}{da_1} = [\beta_1\beta_2 (\mathbf{n}_2 \otimes \mathbf{r}_{12}) \psi(s) da_2] \cdot \mathbf{n}_1 \tag{26}$$

$$\frac{d\mathbf{F}_2}{da_2} = [\beta_1\beta_2 (\mathbf{n}_1 \otimes \mathbf{r}_{21}) \psi(s) da_1] \cdot \mathbf{n}_2 \tag{27}$$

Define

$$\mathbf{t}_I^s := \frac{d\mathbf{F}_I}{da_I}, \quad \boldsymbol{\sigma}_I^s := \beta_I \beta_J (\mathbf{n}_J \otimes \mathbf{r}_{IJ}) \psi(s) da_J, \quad I, J = 1, 2, I \neq J \tag{28}$$

and Eq. (26) and (27) can then be written as

$$\mathbf{t}_I^s = \boldsymbol{\sigma}_I^s \mathbf{n}_I \tag{29}$$

where $\boldsymbol{\sigma}_I^s$ and $\mathbf{t}_I^s$ are the surface stress tensor and the corresponding traction force on $\partial\Omega_I$

Remark 1.
1. From Eq. (22), one can see that $d\mathbf{F}_1$ is in the direction of $\mathbf{n}_2$, i.e., the contact force applying on da_1 due to the presence of da_2 is in the unit out normal of $\partial\Omega_2$ at the point of interest, which indicates that the contact interaction here is frictionless.
2. In general, $d\mathbf{F}_1 \neq -d\mathbf{F}_2$, but the total force applying on body Ω_1 due to the presence of body Ω_2 is equal to that acting on body Ω_2 due to the presence of body Ω_1, i.e., $\sum d\mathbf{F}_1 = \sum d\mathbf{F}_2$, as one would expect from Newton's third law.
3. In addition, the contact force $d\mathbf{F}_1$ can also be viewed as the integral of the negative gradient of the following surface potential,

$$\Pi^{C,s} = \int_{\partial\Omega_1} \int_{\partial\Omega_2} \beta_1 \beta_2 u(s) (\mathbf{n}_1 \cdot \mathbf{n}_2) da_1 da_2 \tag{30}$$

where s is the distance between the points from the two surfaces, and $u(s)$ is the potential defined as

$$u(s) = \int \psi(s) s ds \,. \tag{31}$$

4. Galerkin weak form of the adhesive contact model

In this section, the Galerkin weak form formulation of the proposed multiscale contact model shall be presented. Consider the continuum system shown in Fig. 1, the total kinetic energy of the system can be written as

$$K^{tot} = \sum_{I=1}^{2} K^I = \sum_{I=1}^{2} \int_{\Omega_I} \frac{1}{2} \rho_I \mathbf{v}_I^2 dv_I, \tag{32}$$

where ρ_I and $\mathbf{v}_I = \dot{\mathbf{u}}_I$ are the mass density and velocity field in the body Ω_I, $I = 1, 2$, respectively. The total Lagrangian of the system is given by

$$\mathcal{L} = \Pi^{tot} - K^{tot}, \tag{33}$$

where K^{tot} and Π^{tot} are the total kinetic energy and potential energy of the system, respectively. The Hamilton principle requires that the action

$$\mathcal{S} = \int_{t_1}^{t_2} \mathcal{L} dt \tag{34}$$

attains its stationary value for true solution, that is $\delta\mathcal{S} = 0$ holds for all kinematically admissible variations:

$$\begin{aligned} \delta\mathcal{S} &= \int_{t_1}^{t_2} \delta\mathcal{L} dt = 0 \\ &= \int_{t_1}^{t_2} \left\{ \sum_{I=1}^{2} \left[\delta\Pi^{int,I} + \delta\Pi^{ext,I} - \delta K^I \right] + \delta\Pi^{C,s} \right\} dt, \quad \forall \delta\mathbf{u}_I \end{aligned} \tag{35}$$

The first variation of the kinetic energy for body Ω_I is given by

$$\delta K^I = \int_{\Omega_I} \rho_I \mathbf{v}_I \cdot \delta\mathbf{v}_I dv_I. \tag{36}$$

By using integration by parts,

$$\int_{t_1}^{t_2} \rho_I \mathbf{v}_I \cdot \delta\mathbf{v}_I dt = (\rho_I \mathbf{v}_I \delta\mathbf{u}_I)_{t_1}^{t_2} - \int_{t_1}^{t_2} \rho_I \dot{\mathbf{v}}_I \delta\mathbf{u}_I dt = -\int_{t_1}^{t_2} \rho_I \dot{\mathbf{v}}_I \delta\mathbf{u}_I dt, \tag{37}$$

where $\delta\mathbf{u}_I$ is chosen to be zero at time t_1 and t_2. By switching the order of integration, one can obtain,

$$\int_{t_1}^{t_2} \delta K^I dt = \int_{t_1}^{t_2} \int_{\Omega_I} \rho_I \mathbf{v}_I \cdot \delta\mathbf{v}_I dv_I dt = -\int_{t_1}^{t_2} \int_{\Omega_I} \rho_I \dot{\mathbf{v}}_I \delta\mathbf{u}_I dv_I dt \tag{38}$$

Following the derivation in Section 3, one may see that the first variation of the contact interaction energy $\Pi^{C,s}$ can be expressed as

$$\delta\Pi^{C,s} = \int_{\partial\Omega_1} \int_{\partial\Omega_2} \beta_1\beta_2 [(\mathbf{n}_2 \otimes \mathbf{r}_{12}) \cdot \mathbf{n}_1 \psi(s) \cdot \delta\mathbf{u}_1 + \mathbf{n}_1 \otimes \mathbf{r}_{21}) \cdot \mathbf{n}_2 \psi(s) \cdot \delta\mathbf{u}_2] da_2 da_1. \tag{39}$$

Since Eq. (35) is valid for all nodal virtual displacements $\delta\mathbf{u}_I$, the expression inside the bracket should be equal to zero, that is,

$$\sum_{I=1}^{2} \left[\int_{\Omega_I} \rho_I \dot{\mathbf{v}}_I \delta\mathbf{u}_I dv_I + \int_{\Omega_I} \boldsymbol{\sigma}_I : \frac{\partial \delta\mathbf{u}_I}{\partial \mathbf{x}_I} dv_I \right] + \int_{\partial\Omega_1} \int_{\partial\Omega_2} \beta_1\beta_2 [(\mathbf{n}_2 \otimes \mathbf{r}_{12}) \cdot \mathbf{n}_1 \psi(s) \cdot \delta\mathbf{u}_1 + (\mathbf{n}_1 \otimes \mathbf{r}_{21}) \cdot \mathbf{n}_2 \psi(s) \cdot \delta\mathbf{u}_2] da_2 da_1 = \sum_{I=1}^{2} \left[\int_{\Omega_I} \rho_I \mathbf{b}_I \cdot \delta\mathbf{u}_I dv_I + \int_{\partial\Omega_{IT}} \mathbf{t}_I \cdot \delta\mathbf{u}_I ds \right], \quad \forall \delta\mathbf{u}_I, I = 1, 2 \tag{40}$$

This is the Galerkin weak form of the multiscale adhesive contact model.

5. Computational algorithm and computer implementation

In this section, using standard FEM method, e.g. [27,28], we discretize the weak form of Eq. (40), from which the global mass matrix, internal force vector, external force vector, and the contact force vector are identified. The computational algorithms and the computer implementation details for both quasi-static and explicit dynamic simulations are presented below.

Consider the following interpolations of the displacement field $\mathbf{u}_I$ and the corresponding variation $\delta\mathbf{u}_I$ for body Ω_I,

$$\mathbf{u}_I(\mathbf{x}) = \sum_{A=1}^{n_{node}} N_I^A(\mathbf{x}) \mathbf{d}_I^A, \quad I = 1, 2 \tag{41}$$

and

$$\delta\mathbf{u}_I(\mathbf{x}) = \sum_{A=1}^{n_{node}} N_I^A(\mathbf{x}) \delta\mathbf{d}_I^A, \quad I = 1, 2 \tag{42}$$

where n_{node} denotes the number of nodes in the system, $N^A(\mathbf{x})$ is the finite element shape function associated with node A, and $\mathbf{d}_I^A$ and $\delta\mathbf{d}_I^A$ are the displacement and the corresponding virtual displacement at node A. In practical application, Eq. (41) and (42) are expressed element-wisely, i.e.,

$$\mathbf{u}_I(\mathbf{x})|_{\Omega_I^e} = \sum_{A=1}^{n_{en}} N_I^A(\mathbf{x}) \mathbf{d}_I^A \quad I = 1, 2 \tag{43}$$

and

$$\delta\mathbf{u}_I(\mathbf{x})|_{\Omega_I^e} = \sum_{A=1}^{n_{en}} N_I^A(\mathbf{x}) \delta\mathbf{d}_I^A \quad I = 1, 2 \tag{44}$$

where n_{en} is the number of nodes for each element.

Substituting Eq. (43) and (44) into Eq. (40) and reorganizing different terms, one may obtain

$$\sum_{I=1}^{2}\sum_{iel=1}^{n_{elem}}\sum_{A=1}^{n_{en}}\sum_{B=1}^{n_{en}}\delta\mathbf{d}_I^A\cdot\int_{\Omega_I^e}\rho_I N_I^A N_I^B\ddot{\mathbf{d}}_I^B dv_I+\sum_{I=1}^{2}\sum_{iel=1}^{n_{elem}}\sum_{A=1}^{n_{en}}\delta\mathbf{d}_I^A\cdot\int_{\Omega_I^e}\boldsymbol{\sigma}_I\frac{\partial N_I^A}{\partial\mathbf{x}_I}dv_I$$
$$-\sum_{I=1}^{2}\sum_{iel=1}^{n_{elem}}\sum_{A=1}^{n_{en}}\delta\mathbf{d}_I^A\cdot\int_{\Omega_I^e}\rho_I N_I^A\mathbf{b}_I dv_I-\sum_{I=1}^{2}\sum_{iel=1}^{n_{elem}}\sum_{A=1}^{n_{en}}\delta\mathbf{d}_I^A\cdot\int_{\partial\Omega_{TI}^e}N_I^A\mathbf{t}_I ds_I$$
$$+\sum_{I=1}^{2}\sum_{isel=1}^{n_{selem1}}\sum_{jsel=1}^{n_{selem2}}\sum_{A=1}^{n_{sen}}\int_{\partial\Omega_1^e}\int_{\partial\Omega_2^e}\beta_1\beta_2 N_I^A(\mathbf{n}_J\otimes\mathbf{r}_{IJ})\cdot\mathbf{n}_I\psi(s)da_2da_1,\quad I=1,2 \tag{45}$$

which is essentially

$$\delta\mathbf{d}_I\cdot\left(\mathbf{M}_I\ddot{\mathbf{d}}_I+\mathbf{f}_I^{int}+\mathbf{f}_I^{cont}-\mathbf{f}_I^{ext}\right)=0,\quad I=1,2 \tag{46}$$

where we have defined the following quantities

$$\mathbf{M}_I=\sum_{iel=1}^{n_{elem}}\sum_{A=1}^{n_{en}}\sum_{B=1}^{n_{en}}\int_{\Omega_I^e}\rho_I N_I^A N_I^B dv_I \tag{47}$$

$$\mathbf{f}_I^{int}=\sum_{iel=1}^{n_{elem}}\sum_{A=1}^{n_{en}}\int_{\Omega_I^e}\boldsymbol{\sigma}_I\frac{\partial N_I^A}{\partial\mathbf{x}_I}dv_I \tag{48}$$

$$\mathbf{f}_I^{ext}=\sum_{iel=1}^{n_{elem}}\sum_{A=1}^{n_{en}}\int_{\Omega_I^e}\rho_I N_I^A\mathbf{b}_I dv_I+\sum_{iel=1}^{n_{elem}}\sum_{A=1}^{n_{en}}\int_{\partial\Omega_{TI}^e}N_I^A\mathbf{t}_I ds_I \tag{49}$$

$$\mathbf{f}_I^{cont}=\sum_{isel=1}^{n_{selem1}}\sum_{jsel=1}^{n_{selem2}}\sum_{A=1}^{n_{sen}}\int_{\partial\Omega_1^e}\int_{\partial\Omega_2^e}\beta_1\beta_2 N_I^A(\mathbf{n}_J\otimes\mathbf{r}_{IJ})\cdot\mathbf{n}_I\psi(s)da_2da_1,\ I,J=1,2,\ I\neq J, \tag{50}$$

in which, n_{selem1} and n_{selem2} are the total number of surface elements on $\partial\Omega_1$ and $\partial\Omega_2$, respectively, n_{sen} is the number nodes for each surface element, $\mathbf{n}_I$ and $\mathbf{n}_J$ are the unit surface out-normal at corresponding surface points $\mathbf{r}_I\in\partial\Omega_I$ and $\mathbf{r}_J\in\partial\Omega_J$, and $\mathbf{r}_{IJ}=\mathbf{r}_I-\mathbf{r}_J$ is the vector pointing from $\mathbf{r}_I$ to $\mathbf{r}_J$. Due to the arbitrariness of the variation $\delta\mathbf{d}_I$, Eq. (46) can be reduced to

$$\mathbf{M}_I\ddot{\mathbf{d}}_I+\mathbf{f}_I^{int}+\mathbf{f}_I^{cont}-\mathbf{f}_I^{ext}=\mathbf{0},\quad I=1,2 \tag{51}$$

which is the discretized equations of motion of the system.

Define the resultant force vector

$$\mathbf{f}_I(\mathbf{d})=\mathbf{f}_I^{ext}(\mathbf{d}_I)-\mathbf{f}_I^{int}(\mathbf{d}_I)-\mathbf{f}_I^{cont}(\mathbf{d}_1,\mathbf{d}_2),\quad I=1,2 \tag{52}$$

and then the discretized equations of motion in Eq. (51) can be written as

$$\mathbf{M}_I\ddot{\mathbf{d}}_I=\mathbf{f}_I(\mathbf{d}),\quad I=1,2 \tag{53}$$

5.1. Implementation: quasi-static case

For the quasi-static case, we have $\ddot{\mathbf{d}}_I=\mathbf{0}$ and the static equilibrium is simply governed by the nonlinear equation for each body Ω_I

$$\mathbf{f}_I(\mathbf{d})=\mathbf{0},\quad I=1,2 \tag{54}$$

This type of equation can only be solved approximately. One may notice that the contact interaction force $\mathbf{f}_1^{cont}$ and $\mathbf{f}_2^{cont}$ both depend on the two displacement vectors $\mathbf{d}_1$ and $\mathbf{d}_2$ of the two interaction bodies, which is expected as they are coupled. Thus we have to solve the displacement fields in the two bodies simultaneously. In this respect, we rewrite Eq. (54) as

$$\mathbf{f}(\mathbf{d})=\mathbf{f}^{ext}-\mathbf{f}^{int}(\mathbf{d})-\mathbf{f}^{cont}(\mathbf{d})=\mathbf{0} \tag{55}$$

where $\mathbf{d} = [\mathbf{d}_1; \mathbf{d}_2]$, $\mathbf{f}(\mathbf{d}) = [\mathbf{f}_1(\mathbf{d}); \mathbf{f}_2(\mathbf{d})]$, $\mathbf{f}^{ext}(\mathbf{d}) = [\mathbf{f}_1^{ext}(\mathbf{d}_1); \mathbf{f}_2^{ext}(\mathbf{d}_2)]$, $\mathbf{f}^{int}(\mathbf{d}) = [\mathbf{f}_1^{int}(\mathbf{d}_1); \mathbf{f}_2^{int}(\mathbf{d}_2)]$, and $\mathbf{f}^{cont}(\mathbf{d}) = [\mathbf{f}_1^{cont}(\mathbf{d}); \mathbf{f}_2^{cont}(\mathbf{d})]$. Under the condition of dead external load, that is $\mathbf{f}^{ext}(\mathbf{d})$ is independent of the displacement field $\mathbf{d}$, the whole system is conservative and we can employ the famous Newton–Raphson method [31] to solve Eq. (55).

To apply the Newton–Raphson method, for each iteration step in a load step, we not only need to compute all the force vectors, but also the tangent stiffness matrices related to the displacement dependent force vectors. For the calculation of the external and internal force vectors ($\mathbf{f}^{ext}$ and $\mathbf{f}^{int}$), as well as the stiffness matrix $\mathbf{K}^{int} = \frac{\partial \mathbf{f}^{int}}{\partial \mathbf{d}}$, we refer to the nonlinear finite element literature [2,31]. Instead, we are going to focus on the computation of the contact interaction force vector. A detailed derivation of the contact stiffness matrix is provided in Appendix A.

In practice, the global force vectors or matrices are assembled from element force vectors and matrices. For the contact problem, we shall consider the contact interaction from surface elements from the two bodies Ω_i^e and Ω_j^e. Obviously, if the two elements are from the same body, say Ω_1, then there would be no contact interaction, and hence no contribution to the contact force vector or matrix. Thus we introduce the following characteristic function

$$\chi(\Omega_i^e, \Omega_j^e) = \begin{cases} 0, & \text{if elements } i \text{ and } j \text{ belong to the same body} \\ 1, & \text{if elements } i \text{ and } j \text{ belong to different bodies} \end{cases} \tag{56}$$

With this characteristic function, the element contact interaction force vectors acted on element $\partial\Omega_i^e$ and $\partial\Omega_j^e$ can be written as

$$\mathbf{fe}_{ij}^{cont,i} = \int_{\partial\Omega_i^e} \int_{\partial\Omega_j^e} \chi(\Omega_i^e, \Omega_j^e) \beta_i \beta_j \mathbf{N}^i (\mathbf{n}_j \otimes \mathbf{r}_{ij}) \cdot \mathbf{n}_i \psi(s) da_j da_i \tag{57}$$

and

$$\mathbf{fe}_{ij}^{cont,j} = \int_{\partial\Omega_i^e} \int_{\partial\Omega_j^e} \chi(\Omega_i^e, \Omega_j^e) \beta_i \beta_j \mathbf{N}^j (\mathbf{n}_i \otimes \mathbf{r}_{ji}) \cdot \mathbf{n}_j \psi(s) da_j da_i \tag{58}$$

where $\mathbf{n}_i$ and $\mathbf{n}_j$ are the unit surface out-normals at surface points $\mathbf{r}_i$ and $\mathbf{r}_j$, respectively, $\mathbf{r}_{ij} = \mathbf{r}_i - \mathbf{r}_j$ is the relative position vector with length $s = \|\mathbf{r}_{ij}\|$, $\psi(s)$ is the function defined in Eq. (21) and $\mathbf{N}^i$, $\mathbf{N}^j$ denote the shape function for element i and element j, respectively. The shape function for a generic element with n_{en} nodes can be written in matrix form as

$$\mathbf{N} = \left[N^1 \mathbf{1}, N^2 \mathbf{1}, \ldots, N^{n_{en}} \mathbf{1} \right] \tag{59}$$

in which, $\mathbf{1}$ is the identity matrix and N^A, $A = 1, 2, \ldots, n_{en}$ is the value of the shape function at each node A.

By using the Nanson's formula $\mathbf{n}da = J\mathbf{F}^{-T}\mathbf{N}dA$ and noticing $\beta_{i0} = J\beta_i$, $\beta_{j0} = J\beta_j$, one can convert them into the reference configuration as

$$\mathbf{fe}_{ij}^{cont,i} = \int_{\partial\Omega_i^{e0}} \int_{\partial\Omega_j^{e0}} \chi(\Omega_i^e, \Omega_j^e) \beta_{i0} \beta_{j0} \mathbf{N}^i \left[(\mathbf{F}_j^{-T} \mathbf{N}_j) \otimes \mathbf{r}_{ij} \right] \cdot (\mathbf{F}_i^{-T} \mathbf{N}_i) \psi(r) dA_i dA_j \tag{60}$$

and

$$\mathbf{fe}_{ij}^{cont,j} = \int_{\partial\Omega_i^{e0}} \int_{\partial\Omega_j^{e0}} \chi(\Omega_i^e, \Omega_j^e) \beta_{i0} \beta_{j0} \mathbf{N}^j \left[(\mathbf{F}_i^{-T} \mathbf{N}_i) \otimes \mathbf{r}_{ji} \right] \cdot (\mathbf{F}_j^{-T} \mathbf{N}_j) \psi(r) dA_i dA_j \tag{61}$$

where $\mathbf{N}_i$, $\mathbf{N}_j$ and $\mathbf{F}_i$, $\mathbf{F}_j$ denote the initial unit surface out-normals and the deformation gradient tensors at the points of interest. Notice that the meaning of $\mathbf{N}^i$ and $\mathbf{N}_i$ are completely different.

As one may notice, the evaluations of the contact interaction forces expressed in Eqs. (60) and (61) require the unit out-normals ($\mathbf{N}_1$ and $\mathbf{N}_2$) in the reference configuration. The computational formula to obtain these out-normals for an arbitrarily shaped body is provided in Appendix B.

The algorithm flow chart for quasi-static analysis of the proposed contact model is shown in Table 1.

5.2. Implementation: dynamic case

In the dynamic case, one has to evaluate acceleration of the displacement field. For the sake of simplicity, the following lumped mass matrix is employed in transient analysis

$$\mathbf{M}_I = \sum_{iel=1}^{n_{elem}} \sum_{A=1}^{n_{en}} \int_{\Omega_i^e} \rho_I N_I^A \mathbf{1} dv_I, \quad I = 1, 2 \tag{62}$$

Table 1
Solution algorithm for the quasi-static analysis of the proposed contact formulation.

Loading loop: apply load in increments, e.g., prescribed forces and displacements
Newton–Raphson iteration: to obtain the solution displacement of Eq. (55)
- provide an initial guess $\mathbf{u}_0$, e.g., set $\mathbf{u}_0 = \mathbf{0}$ at first load step
  or based on the solution of the previous load step.
- iterate until convergence: (energy residual $\mathbf{K}_{tot}^T \Delta\mathbf{u} < TOL$)
  1. loop over the volume elements Ω_e to compute $\mathbf{fe}^{int}$ and $\mathbf{ke}^{int}$
     assemble them into the global force vector $\mathbf{f}_{tot}$ and stiffness matrix $\mathbf{K}_{tot}$
  2. double loop over the surface elements to compute $\mathbf{fe}^{cont}$ and $\mathbf{ke}^{cont}$
     (1). compute $\mathbf{ke}^{cont}$ and $\mathbf{fe}^{cont}$
     (2). assemble $\mathbf{fe}^{cont}$ and $\mathbf{ke}^{cont}$ into $\mathbf{f}_{tot}$ and $\mathbf{K}_{tot}$
  3. impose the boundary condition
  4. solve $\mathbf{K}_{tot}\Delta\mathbf{u} = -\mathbf{f}_{tot}$
  5. update $\mathbf{u}_{i+1} = \mathbf{u}_i + \Delta\mathbf{u}$

Table 2
Solution algorithm for the explicit dynamic analysis of the proposed contact formulation.

Preprocess: compute the mass matrix $\mathbf{M}$, initialize the displacement $\mathbf{u}_0$, velocity $\mathbf{v}_{-1/2}$ and acceleration $\mathbf{a}_0$
time loop: at each time step
1. compute the half step velocity $\mathbf{v}_{n+\frac{1}{2}}$ by $\mathbf{v}_{n+\frac{1}{2}} = \mathbf{v}_{n-\frac{1}{2}} + \frac{1}{2}\mathbf{a}_n\Delta t$
2. compute the full step displacement $\mathbf{d}_{n+1}$ by $\mathbf{d}_{n+1} = \mathbf{d}_n + \mathbf{v}_{n+\frac{1}{2}}\Delta t$
3. prescribe the essential boundary conditions; e.g., displacement boundary condition
4. loop over the volume elements Ω_e to compute $\mathbf{fe}^{int}$
   assemble $\mathbf{fe}^{int}$ into the global force vector $\mathbf{f}_{tot}$
5. double loop over the surface elements to compute $\mathbf{fe}^{cont}$
   (1). compute $\mathbf{fe}^{cont}$ are based on Eq. (60) and (61)
   (2). assemble $\mathbf{fe}^{cont}$ into $\mathbf{f}_{tot}$
6. compute the full step velocity $\mathbf{v}_{n+1} = \mathbf{v}_{n+\frac{1}{2}} + \frac{1}{2}\Delta t\mathbf{a}_{n+1}$, if needed.

where $\mathbf{1}$ is the identity matrix of dimension *ndim* by *ndim*. By using central difference method in the time integration, the algorithm flow chart for the explicit dynamic analysis is shown in Table 2.

6. Numerical examples and discussions

In this section, we present three numerical examples, in which the proposed surface formulation is employed to solve the adhesive contact mechanics problems.

6.1. Example: an indentation problem

To test the numerical performance of the proposed surface contact formulation, the following model problem is investigated. Consider the problem of a cylinder, with radius R_0, located above the half space, which are pushed together by a displacement u, as shown in Fig. 3(a). The half-space is modeled by a block of size $5R_0 \times 10R_0$, such that there would be no spurious boundary effects. An initial gap of $g_0(u) = 0.2R_0$ exists between the half space and the lowest point of the cylinder. In the simulation, the cylinder and the half-space are both modeled by the hyperelastic Neo-Hookean material with Young's modulus E_0 and Possion's ratio $\nu = 0.2$. The contact interacting parameters are set to be $\sigma_0 = 0.1R_0$, $\epsilon = \frac{3}{2}\beta_0^2 R_0^3$. The cylinder is pushed down by the relative displacement u, which causes the resultant reaction force $P(u)$ in the vertical direction. For simplicity, the problem is considered in the state of plane strain. A quasi-static analysis of the problem is conducted by FEM. The model is discretized into 588 nodes and 534 quadrilateral elements, as shown in Fig. 3(b). Notice that the mesh is refined at the contact region, so as to reduce the computational cost.

In the simulation, a set of reduced units is used. The radius of the cylinder R_0, Young's modulus E_0 of the Neo-Hookean material, and the particle density β_0 of both material are selected to be the three basic units. The unit of stress is represented by E_0/R_0^3. Both the volume and surface integration methods are used in this quasi-static model problem. For both methods, the indenter vertical advance step size is chosen as $0.01R_0$ in the simulation. To make sure the stability and accuracy, we use 5×5 quadrature points in the volume integral method, and 5 quadrature points in surface integration method. The deformed mesh and the stress $I_1 = \mathrm{tr}(\boldsymbol{\sigma})$ is shown in Fig. 4 for $u = R_0$. It can be seen that the deformations are mainly concentrated in the refined region. The resultant reaction force $P(u)$ and the gap between the cylinder and the half space $g(u)$ are shown in Fig. 5. One can see that there are small margins for both curves of the two methods. This can be attributed to the following reasons. In the numerical computation, the contact interaction forces are obtained through the integration of the Gauss quadrature points. For the volume integration based method, no matter how small the size of the element is, one can never have a quadrature point located on the surface of the bulk element. On the other hand, surface integral method obtains the interaction force based on quadrature points on the surface element. With the same macro configurations e.g. positions of the two macro bodies, meshes, etc., the surface integration method would provide

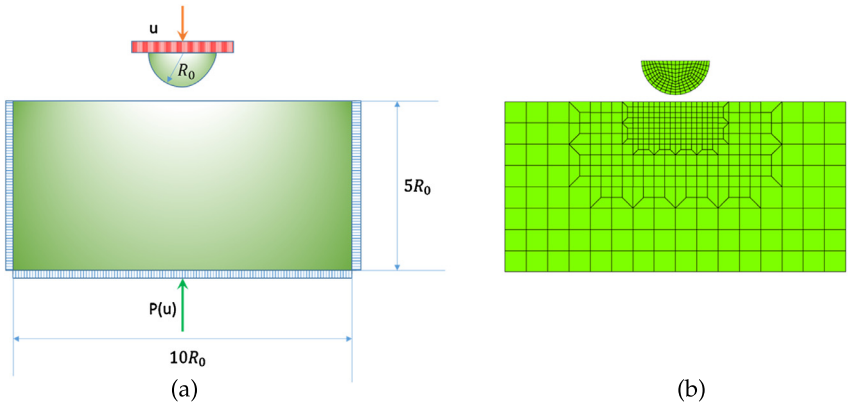

Fig. 3. The model indentation problem. (a) Geometry and boundary conditions. (b) FEM mesh.

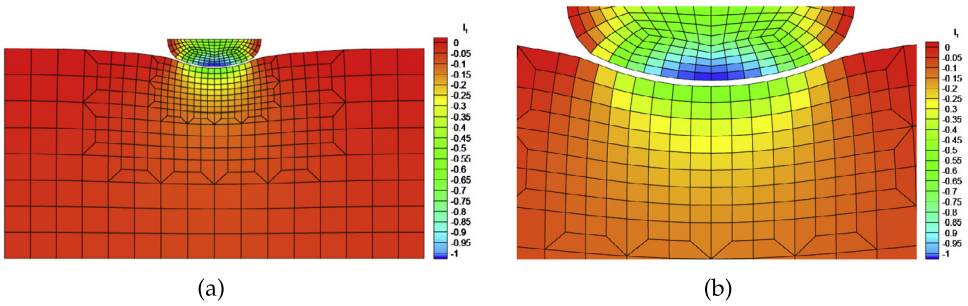

Fig. 4. Stress distribution. (a) Stress $I_1 = \mathrm{tr}(\boldsymbol{\sigma})$ at load step $u = R_0$. (b) Enlargement of the refined region.

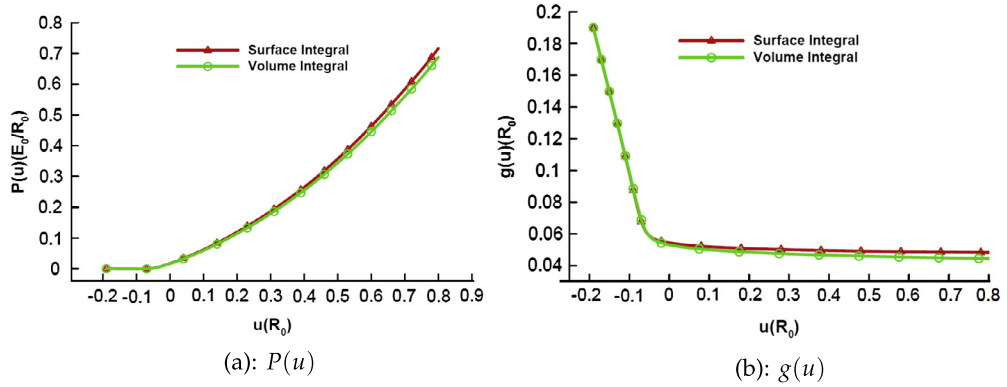

Fig. 5. Main results of the indentation problem: (a) The resultant reaction force $P(u)$ versus the prescribed displacement; (b) The gap $g(u)$ versus the prescribed displacement.

larger repulsive forces, because the distance between two integration points from two macro bodies are much closer. If one does not consider the errors from interpolations, i.e., the approximation of the curvy edges, the surface integral shall provide a better approximation of the interaction force, due to the fact that the main contributions of the interaction forces between the two interacting bodies comes from particles with the closer distances, particularly from particles located on the surface.

To check the rate of convergence of the proposed surface formulation, five successive meshes with the mesh sizes of $h_1 = 0.625R_0$, $h_2 = 0.3125R_0$, $h_3 = 0.15625R_0$, $h_4 = 0.078125R_0$ and $h_5 = 0.0390625R_0$ are generated. The meshes for the case of h_1 and h_4 are shown in Fig. 6. By treating the finest mesh of h_5 as the 'exact' solution, the following relative error $e(f)$ of a generic quantity $f(h)$ is defined as

$$e(f) := \left\| \frac{f(h) - f(h_5)}{f(h_5)} \right\| . \tag{63}$$

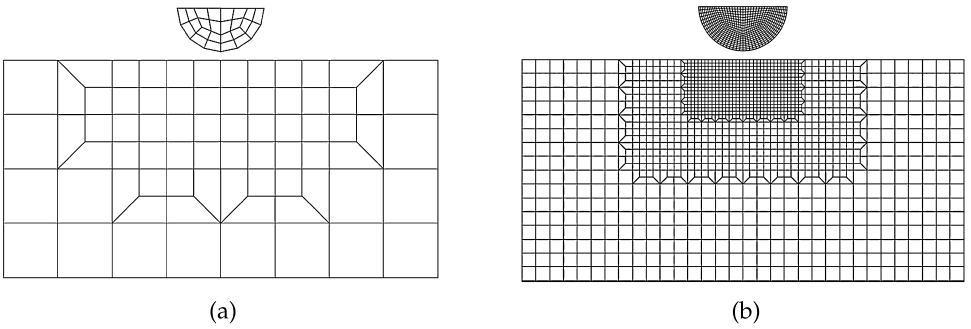

Fig. 6. Different meshes for convergence study. (a) Coarse mesh. (b) Fine mesh.

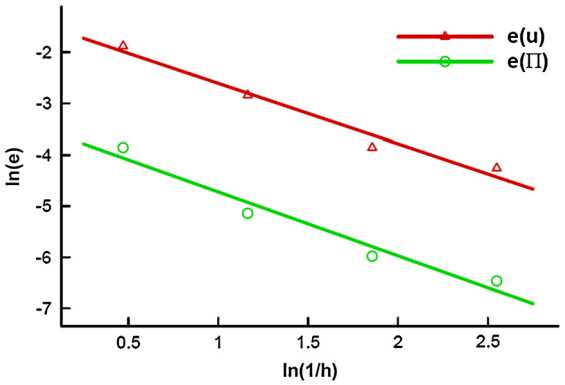

Fig. 7. Convergence of the FEM solution. loglog plots of the relative errors $e(u)$ and $e(\Pi)$. The slopes of the two curves are $n_1 = -1.06$ and $n_2 = -1.12$.

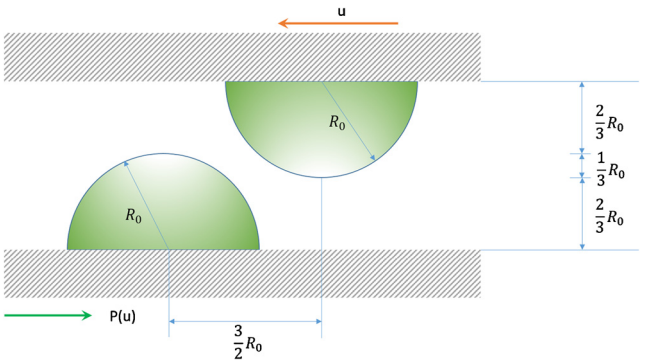

Fig. 8. Sliding contact: geometry of the two sliding half spheres.

Two quantities are checked, the vertical displacement $u(h)$ at the top middle point of the block and the total potential energy of the system $\Pi(h)$ (internal elastic energy and the contact interaction energy). Fig. 7 shows the loglog plot of relative errors for both of them. One can easily see that both results are convergent. Linear fittings of the two curves yield the slopes of $n_1 = -1.06$ for $e(u)$ and $n_2 = -1.12$ for $e(\Pi)$, revealing that the proposed method is approximately of first order accuracy with respect to the mesh size.

6.2. Example: frictionless sliding

In this example, we present a numerical simulation of applying the adhesive contact model to study the frictionless sliding contact between two half spheres as shown in Fig. 8. This idealized contact model can happen between the rough surfaces of two macro bodies. The two half spheres are both modeled as hyperelastic Neo-Hookean materials [32], with Young's modulus E_0 and Possion's ratio $\nu = 0.2$. The radius of the sphere is R_0 and the corresponding contact interacting parameters are provided as $\sigma_0 = 0.15R_0$, $\epsilon = \frac{3}{2}\beta_0^2 R_0^3$. As a comparison, quasi-static simulations are carried out for both the method developed here and the volume integral based approach proposed in [25].

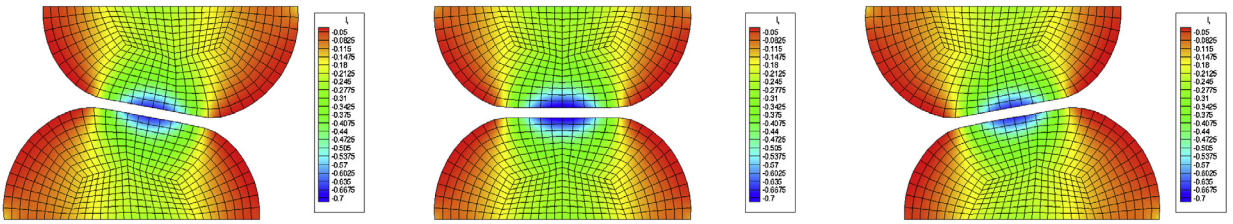

(a): $u = 1.2R_0$ (b): $u = 1.5R_0$ (c): $u = 1.8R_0$

Fig. 9. Sliding contact: I_1 stress distribution of the frictionless sliding of two half spheres.

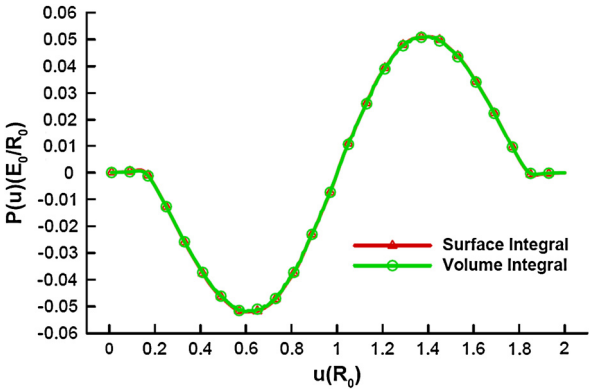

Fig. 10. Horizontal resultant force versus the prescribed displacement. The results are obtained from quasi-static simulations.

Table 3
Computational efficiency of the two methods. The computation is carried out in an Intel Core i7-4700HQ processor with main frequency 2.40 GHz.

	VI, Mesh 1	SI, Mesh 1	VI, Mesh 2	SI, Mesh 2
Number of dofs	684	684	1668	1668
Number of elements (volume/surface)	300	80	768	132
Number of contact pairs	5.6×10^7	1.6×10^5	3.7×10^8	4.4×10^5
CPU time	1.326 s	0.0312 s	7.77 s	0.0936 s

In the simulation, the base of the lower half sphere is fixed with zero displacement and that of the upper half sphere is subjected to an imposed nonzero displacement u in the horizontal direction. The total resultant reaction force at the base of the upper half sphere in the horizontal direction is denoted as P, which is a function of u. Figs. 9(a–c) show the deformation and the pressure ($I_1 = \mathrm{tr}(\boldsymbol{\sigma})$) within the two half spheres, for the case of $u = 0.2R_0, 0.4R_0, 0.6R_0$. The stress and deformation of the two half spheres are symmetric, due to the symmetric contact interaction forces, which is expected. As can be seen, the two asperities are undeformed and stress free at the beginning and the end of the sliding process. Adhesion is a long-range effect characterized by the attractive forces within large separations and repulsive forces at small ones. The relation of the resultant reaction force $P(u)$ versus the prescribed displacement u is shown in Fig. 10, for the both methods. The work required to move the right half sphere can be described by the area between the curve and the u axis. From the two curves in Fig. 10, one can see that during the sliding contact process, attractive forces first dominate, but they are gradually overpowered by the repulsive forces. It can be easily confirmed numerically that the total work for this process is equal to zero and the considered process with the two different formulations is energy conserving, due to the fact that the contact interaction force between the two half spheres is frictionless. However, If dissipative processes are included, e.g. through plastic deformations, the total energy of system is not going to be conserved.

To assess the computation efficiency of the proposed formulation, a comparison study of the two methods in computing the adhesive contact interaction forces and contact tangent stiffness matrix is conducted, and the main comparison parameters are listed in Table 3. Two sets of meshes are used in the comparison simulations. The CPU time denotes the real time that it costs in the computation of the contact forces and stiffness matrix in one single assembling process. It is readily to see that the computation cost of the surface integral method is less than that of the volume integral approach.

6.3. Example: dynamic collision of two cylinders

In this example, we apply the proposed the method to simulate the random collision of two deformable solids in a closed box. In doing so, we hope to demonstrate the ability of the proposed method in simulation of dynamic contact. In specific,

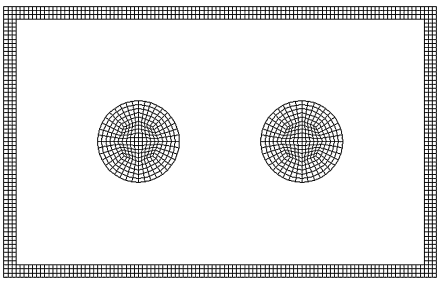

Fig. 11. Impact of two cylinders, discretized by quadrilateral elements.

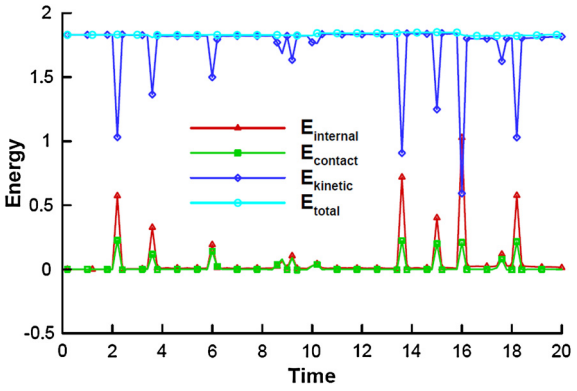

Fig. 12. Energy history for the impact of two cylinders.

we are considering the impact of two hyperelastic cylinders inside a rigid box. The two cylinders are treated in the state of plain strain, with a radius of 1.0 and are discretized with four node quadrilateral elements, as shown in Fig. 11. Notice that a mesh of the rigid wall is needed, for the computation of the contact interaction forces between the cylinders and the wall. The hyperelastic Neo-Hookean material model is assumed for the two cylinders with Young's modulus $E = 1.0 \times 10^3$, Poisson's ratio $\nu = 0.2$, and density $\rho = 1.0$. The contact interaction parameters between any two of the three objects (two cylinders and the wall) are $\beta_1 = \beta_2 = 1.0$, $\sigma_0 = 0.2$ and $\epsilon = 1.5$, with the interaction potential given by Eq. (4). We are interested in energy conservation of the system in a long time simulation. A constant time step $\Delta t = 0.002$ is chosen in the simulation. The left cylinder is given an initial velocity of $v_x = 0.6$, $v_y = -0.9$. The explicit dynamic solution algorithm in Table 2 is employed. The total energy of the system contains three different parts, the kinetic energies and elastic strain energies of the two cylinders and the contact interacting energy among the wall and the cylinders. The time history of the energies is plotted in Fig. 12. As can be seen, the total energy is conserved during the simulation. Figs. 13 and 14 depict the time sequence results. The left cylinder first hits the bottom wall at $t \approx 2.2$, resulting in a decrease of the kinetic energy and an increase of the internal (strain) energy and the contact interaction energy, but the total energy remains at the same level. After bouncing from the wall, the left cylinder impacts the right cylinder at rest, which happens at $t \approx 3.8$, as can be seen from the energy history and the time sequence plot. In fact, each sudden jump of the kinetic energy shown in Fig. 12 indicates an impact, either between a cylinder with the wall or between the two cylinders. Nevertheless, the total energy of the system remains at the same level even after a very long period of simulation. Compared to classic dynamic contact methods in macro scale simulations, here we do not need any enforcement of the non-penetrability condition or other advanced techniques to ensure the conservation of energy [33].

7. Conclusions

In this work, a novel atomistic enriched computational adhesive contact mechanics formulation is developed to study macroscopic interaction between arbitrarily shaped deformable solids. The proposed multiscale adhesive contact mechanics formulation is based on an atomistically induced surface traction formulation, which makes use of the microscopic interaction forces between individual atoms or molecules in the interacting bodies, and then convert the interaction into surface traction. By doing so, the double-layer volume integral describing the contact interaction (energy, force vector, matrix) is reformulated into a double-layer surface integral through a mathematically consistent approach that employs the divergence theorem and a special partitioning technique.

The proposed adhesive contact model is formulated in the framework of continuum mechanics, and its computational formulation is formulated based the Galerkin variational weak formulation. The implementation of computational algorithms is based on the standard finite element discretization, quadrature integration, and time integration for both quasi-static and

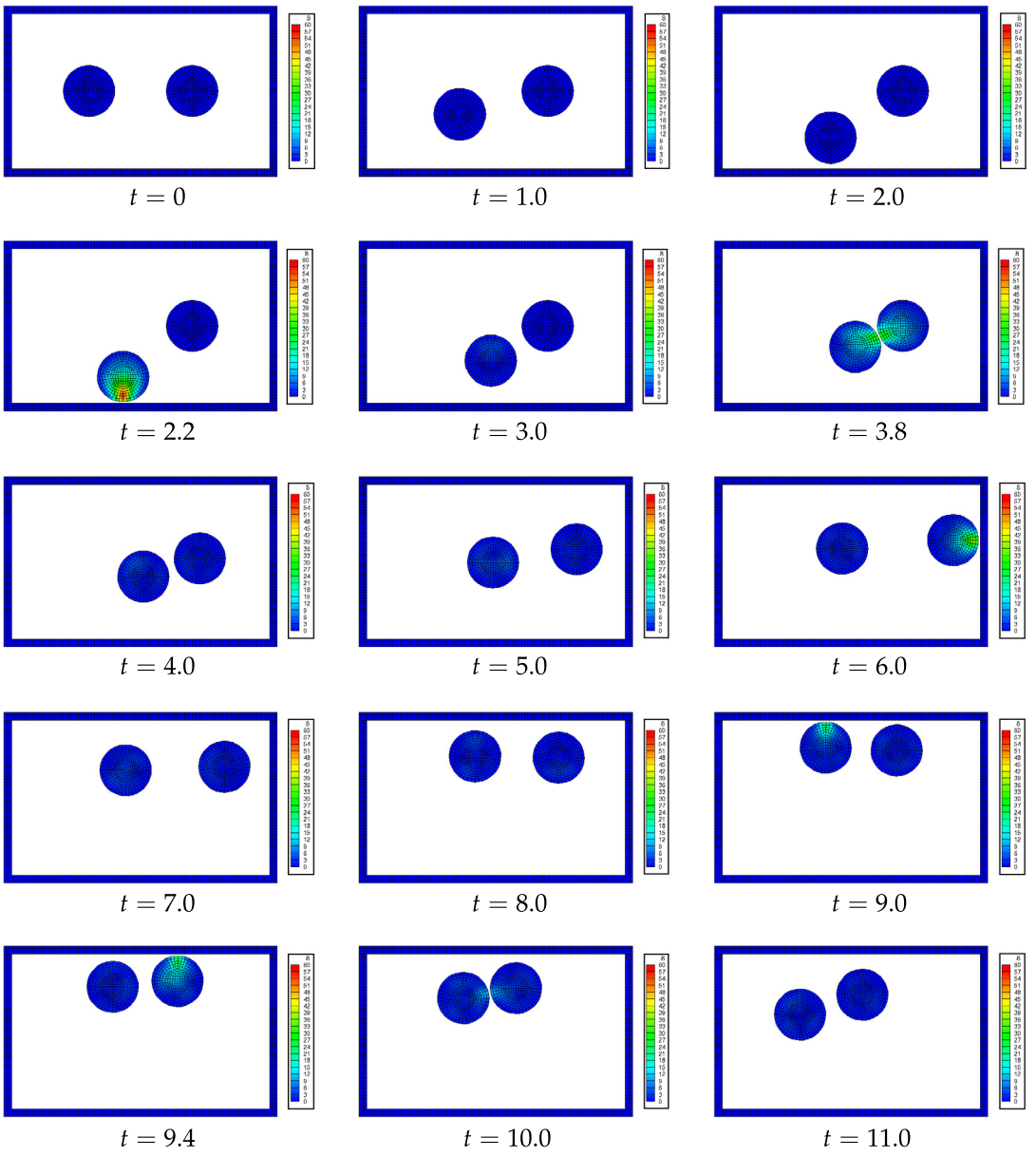

Fig. 13. Time sequence of the impact of two cylinders, $t = 0 \rightarrow 11.0$. The contour shows the instant von Mises stress inside the two cylinder.

dynamic problems. Specially, the contact stiffness matrix corresponding to the adhesive contact interaction force expressed in surface integrals is derived.

Three numerical examples are presented. The first example is a model indentation problem. By conducting quasi-static simulations of the model problem using a series of meshes, it is shown that the proposed method is of first order convergence with respect to the mesh size. The second one is a quasi-static analysis of the frictionless sliding of two half spheres. By comparing to the volume integral approach, it is shown that within the same mesh configuration, the proposed surface approach is faster and more accurate. Because there is no huge penalty constant involved, the stiffness matrix of the system will in general not be ill-conditioned, in contrast to what usually happened in classic penalty based contact method. The third example evolves the dynamic contact/impact of the two cylinders with a rigid wall. It is revealed that the proposed model is energy preserving even in a long time dynamic simulation without any advanced techniques [33].

Acknowledgements

H. Fan was supported by a graduate fellowship from Chinese Scholar Council (CSC), and this support is greatly appreciated.

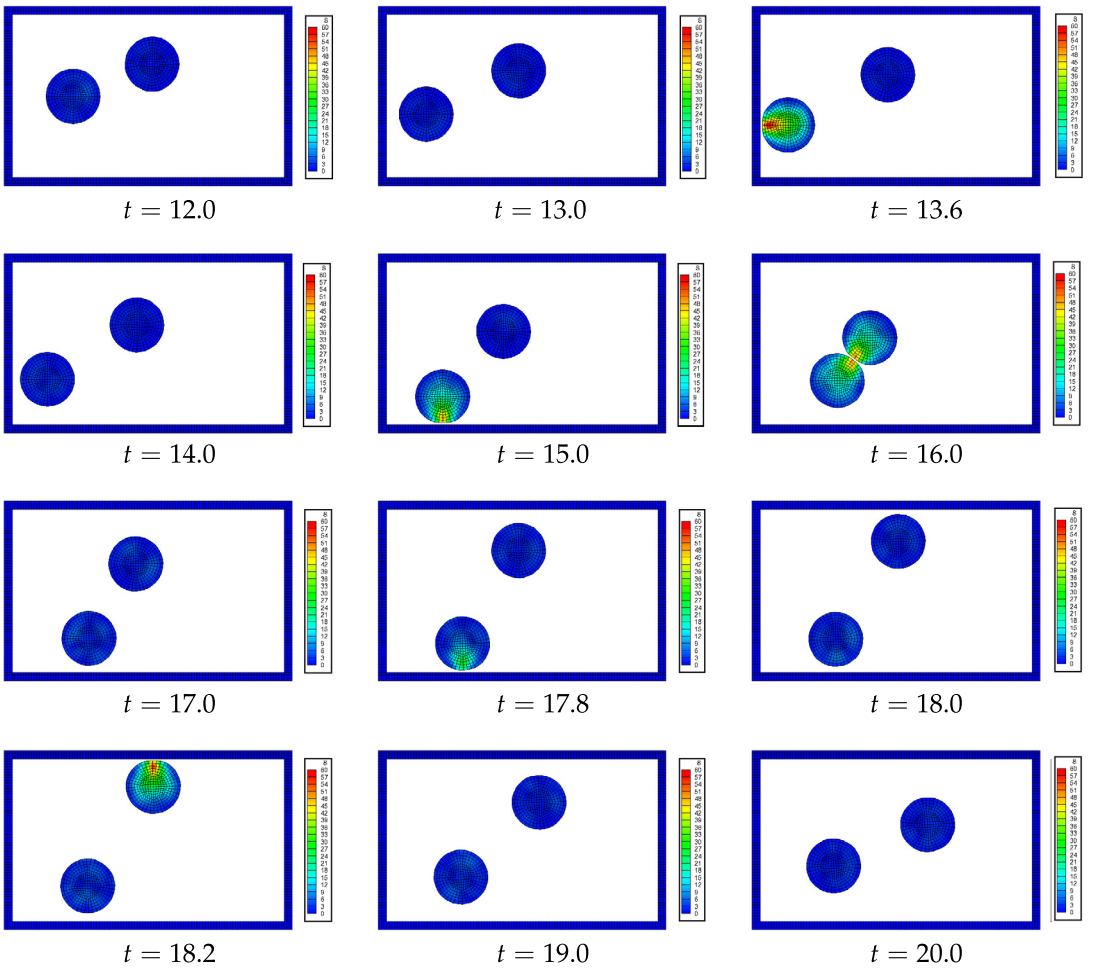

Fig. 14. Time sequence of the impact of two cylinders, $t = 12.0 \rightarrow 20.0$. The contour shows the instant von Mises stress inside the two cylinder.

Appendix A. Tangent stiffness matrix of the contact model

Contribution of the force vector $\mathbf{fe}_{ij}^{cont,i}$ to the element stiffness matrix of Ω_i^e can be obtained by chain rule,

$$\mathbf{ke}^{cont,ii} = \frac{\partial \mathbf{fe}_{ij}^{cont,i}}{\partial \mathbf{u}_i} = \frac{\partial \mathbf{fe}_{ij}^{cont,i}}{\partial \mathbf{x}_i}\mathbf{N}^i \tag{64}$$

where

$$\begin{aligned}\frac{\partial \mathbf{fe}_{ij}^{cont,i}}{\partial \mathbf{x}_i} = &\int_{\partial\Omega_i^{e0}}\int_{\partial\Omega_j^{e0}} \chi(\Omega_i^e,\Omega_j^e)\beta_{i0}\beta_{j0}\mathbf{N}^i(\mathbf{F}_j^{-T}\mathbf{N}_j)\otimes\frac{\partial\left[\mathbf{r}_{ij}\cdot(\mathbf{F}_i^{-T}\mathbf{N}_i)\right]}{\partial\mathbf{x}_i}\psi(r)dA_i dA_j \\ &+\int_{\partial\Omega_i^{e0}}\int_{\partial\Omega_j^{e0}} \chi(\Omega_i^e,\Omega_j^e)\beta_{i0}\beta_{j0}\mathbf{N}^i\left[\mathbf{r}_{ij}\cdot(\mathbf{F}_i^{-T}\mathbf{N}_i)\right](\mathbf{F}_j^{-T}\mathbf{N}_j)\otimes\frac{\partial\psi(r)}{\partial\mathbf{x}_i}dA_i dA_j\end{aligned} \tag{65}$$

in which

$$\frac{\partial\left[\mathbf{r}_{ij}\cdot(\mathbf{F}_i^{-T}\mathbf{N}_i)\right]}{\partial\mathbf{x}_i} = \left(\frac{\partial\mathbf{r}_{ij}}{\partial\mathbf{x}_i}\right)^T(\mathbf{F}_i^{-T}\mathbf{N}_i) + \left(\frac{\partial(\mathbf{F}_i^{-T}\mathbf{N}_i)}{\partial\mathbf{x}_i}\right)^T\mathbf{r}_{ij} \tag{66}$$

and

$$\frac{\partial \psi(r)}{\partial \mathbf{x}_i} = \frac{\partial \psi(r)}{\partial r}\frac{\partial r}{\partial \mathbf{x}_i} = \frac{\partial \psi(r)}{\partial r}\frac{\mathbf{r}_{ij}}{r} \tag{67}$$

The potential function $\psi(r)$ is defined in Eq. (21). In the case of the 12–6 LJ body–body interacting potential $\phi(r)$ defined in Eq. (4), $\psi(r)$ can be obtained as

$$\psi(r) = \frac{2}{3}\epsilon\left[\frac{1}{6}\left(\frac{\sigma_0}{r}\right)^{12} - \left(\frac{\sigma_0}{r}\right)^{6}\right] \tag{68}$$

The corresponding derivative

$$\frac{\partial \psi}{\partial r} = \frac{4\epsilon}{r}\left[-\frac{1}{3}\left(\frac{\sigma_0}{r}\right)^{12} + \left(\frac{\sigma_0}{r}\right)^{6}\right] \tag{69}$$

In Eq. (66),

$$\frac{\partial \mathbf{r}_{ij}}{\partial \mathbf{x}_i} = \mathbf{I} \tag{70}$$

and

$$\left(\frac{\partial(\mathbf{F}_i^{-T}\mathbf{N}_i)}{\partial \mathbf{x}_i}\right)^T \mathbf{r}_{ij} = (\mathbf{r}_{ij}\otimes\mathbf{N}_i) : \frac{\partial \mathbf{F}_i^{-T}}{\partial \mathbf{x}_i} + \left(\frac{\partial \mathbf{N}_i}{\partial \mathbf{x}_i}\right)^T (\mathbf{F}_i^{-1}\mathbf{r}_{ij}) \tag{71}$$

where

$$\frac{\partial \mathbf{N}_i}{\partial \mathbf{x}_i} = \frac{\partial \mathbf{N}_i}{\partial \mathbf{X}_i}\mathbf{F}_i^{-1} \tag{72}$$

The derivative $\frac{\partial \mathbf{F}_i^{-1}}{\partial \mathbf{x}_i}$ can be obtained in the following expressions,

$$\begin{aligned} & F_{Bi}^{-1}F_{iC} = \delta_{BC} \\ \Rightarrow\ & \frac{\partial F_{Bi}^{-1}}{\partial X_A}F_{iC} + F_{Bi}^{-1}\frac{\partial F_{iC}}{\partial X_A} = 0 \\ \Rightarrow\ & \frac{\partial F_{Bi}^{-1}}{\partial X_A} = -F_{Bk}^{-1}\frac{\partial F_{kC}}{\partial X_A}F_{Ci}^{-1} \\ \Rightarrow\ & \frac{\partial F_{Bi}^{-1}}{\partial x_j} = -F_{Bk}^{-1}\mathcal{G}_{kCA}F_{Ci}^{-1}F_{Aj}^{-1} \end{aligned} \tag{73}$$

where

$$\mathcal{G}_{kCA} = \frac{\partial F_{kC}}{\partial X_A} = \frac{\partial^2 x_k}{\partial X_C \partial X_A} \tag{74}$$

Define the matrix

$$\mathbf{K}_{ii}^{s} = (\mathbf{F}_j^{-T}\mathbf{N}_j)\otimes\frac{\partial\left[\mathbf{r}_{ij}\cdot(\mathbf{F}_i^{-T}\mathbf{N}_i)\right]}{\partial \mathbf{x}_i}\psi(r) + \left[\mathbf{r}_{ij}\cdot(\mathbf{F}_i^{-T}\mathbf{N}_i)\right](\mathbf{F}_j^{-T}\mathbf{N}_j)\otimes\frac{\partial \psi(r)}{\partial \mathbf{x}_i} \tag{75}$$

Based on the derivation above, matrix $\mathbf{K}_{ii}^{s}$ can be expressed as

$$\begin{aligned} \mathbf{K}_{ii}^{s} = {} & (\mathbf{F}_j^{-T}\mathbf{N}_j)\otimes\left[\mathbf{F}_i^{-T}\mathbf{N}_i + (\mathbf{r}_{ij}\otimes\mathbf{N}_i) : \frac{\partial \mathbf{F}_i^{-T}}{\partial \mathbf{x}_i} + \mathbf{F}_i^{-T}\left(\frac{\partial \mathbf{N}_i}{\partial \mathbf{X}_i}\right)^T(\mathbf{F}_i^{-1}\mathbf{r}_{ij})\right]\psi(r) \\ & + \left[\mathbf{r}_{ij}\cdot(\mathbf{F}_i^{-T}\mathbf{N}_i)\right]\frac{\partial \psi(r)}{\partial r}\frac{1}{r}(\mathbf{F}_j^{-T}\mathbf{N}_j)\otimes\mathbf{r}_{ij} \end{aligned} \tag{76}$$

The contribution of the force vector $\mathbf{fe}_{ij}^{cont,i}$ to the element stiffness matrix of Ω_i^e can then be written as

$$\mathbf{ke}^{cont,ii} = \int_{\partial\Omega_i^{e0}}\int_{\partial\Omega_j^{e0}} \chi(\Omega_i^e, \Omega_j^e)\beta_{i0}\beta_{j0}\mathbf{N}^i\mathbf{K}_{ii}^{s}\mathbf{N}^i dA_i dA_j \tag{77}$$

Similarly, one can define matrix $\mathbf{K}_{ij}^{s}$, $\mathbf{K}_{jj}^{s}$ and $\mathbf{K}_{ji}^{s}$

$$\mathbf{K}^s_{ij} = \left[\mathbf{r}_{ij}\cdot(\mathbf{F}_i^{-T}\mathbf{N}_i)\right]\psi(r)\left(\mathbf{F}_j^{-T}\frac{\partial \mathbf{N}_j}{\partial \mathbf{X}_j} + \mathbf{N}_j\cdot\frac{\partial \mathbf{F}_j^{-1}}{\partial \mathbf{X}_j}\right)\mathbf{F}_j^{-1} - \psi(r)(\mathbf{F}_j^{-T}\mathbf{N}_j)\otimes(\mathbf{F}_i^{-T}\mathbf{N}_i) + \left[\mathbf{r}_{ij}\cdot(\mathbf{F}_i^{-T}\mathbf{N}_i)\right]\frac{\partial\psi(r)}{\partial r}\frac{1}{r}(\mathbf{F}_j^{-T}\mathbf{N}_j)\otimes\mathbf{r}_{ji} \tag{78}$$

$$\mathbf{K}^s_{jj} = (\mathbf{F}_i^{-T}\mathbf{N}_i)\otimes\left[\mathbf{F}_j^{-T}\mathbf{N}_j + (\mathbf{r}_{ji}\otimes\mathbf{N}_j):\frac{\partial \mathbf{F}_j^{-T}}{\partial \mathbf{x}_j} + \mathbf{F}_j^{-T}\left(\frac{\partial \mathbf{N}_j}{\partial \mathbf{X}_j}\right)^T(\mathbf{F}_j^{-1}\mathbf{r}_{ji})\right]\psi(r) + \left[\mathbf{r}_{ji}\cdot(\mathbf{F}_j^{-T}\mathbf{N}_j)\right]\frac{\partial\psi(r)}{\partial r}\frac{1}{r}(\mathbf{F}_i^{-T}\mathbf{N}_i)\otimes\mathbf{r}_{ji} \tag{79}$$

and

$$\mathbf{K}^s_{ji} = \left[\mathbf{r}_{ji}\cdot(\mathbf{F}_j^{-T}\mathbf{N}_j)\right]\psi(r)\left(\mathbf{F}_i^{-T}\frac{\partial(\mathbf{N}_i)}{\partial \mathbf{X}_i} + \mathbf{N}_i\cdot\frac{\partial \mathbf{F}_i^{-1}}{\partial \mathbf{X}_i}\right)\mathbf{F}_i^{-1} - \psi(r)(\mathbf{F}_i^{-T}\mathbf{N}_i)\otimes(\mathbf{F}_j^{-T}\mathbf{N}_j) + \left[\mathbf{r}_{ji}\cdot(\mathbf{F}_j^{-T}\mathbf{N}_j)\right]\frac{\partial\psi(r)}{\partial r}\frac{1}{r}(\mathbf{F}_i^{-T}\mathbf{N}_i)\otimes\mathbf{r}_{ij} \tag{80}$$

and the other contributions of the force vector $\mathbf{fe}^{cont,i}_{ij}$ and $\mathbf{fe}^{cont,j}_{ij}$ to the element stiffness matrices of Ω^e_i and Ω^e_j become

$$\mathbf{ke}^{cont,ij} = \int_{\partial\Omega^{e0}_i}\int_{\partial\Omega^{e0}_j}\chi(\Omega^e_i,\Omega^e_j)\beta_{i0}\beta_{j0}\mathbf{N}^i\mathbf{K}^s_{ij}\mathbf{N}^j dA_i dA_j \tag{81}$$

$$\mathbf{ke}^{cont,jj} = \int_{\partial\Omega^{e0}_i}\int_{\partial\Omega^{e0}_j}\chi(\Omega^e_i,\Omega^e_j)\beta_{i0}\beta_{j0}\mathbf{N}^j\mathbf{K}^s_{jj}\mathbf{N}^j dA_i dA_j \tag{82}$$

and

$$\mathbf{ke}^{cont,ji} = \int_{\partial\Omega^{e0}_i}\int_{\partial\Omega^{e0}_j}\chi(\Omega^e_i,\Omega^e_j)\beta_{i0}\beta_{j0}\mathbf{N}^j\mathbf{K}^s_{ji}\mathbf{N}^i dA_i dA_j \tag{83}$$

Notice that in general, the contact force vector $\mathbf{ke}^{conts,i}_{ij} \neq \mathbf{ke}^{conts,j}_{ij}$, but $\sum_i^{numelsi}\mathbf{ke}^{cont,i}_{ij} = \sum_j^{numelsj}\mathbf{ke}^{cont,j}_{ij}$. Thus the resulting global contact stiffness matrix is still symmetric.

Appendix B. Initial out-normals of an arbitrarily shaped body

In standard finite element method, an arbitrarily shaped body is discretized into a finite number of sub domains. In three-dimensional space, these sub domains could be tetrahedron, hexahedron, wedge element and so forth. Without loss of generality, let's assume our body is discretized by hexahedrons. In the proposed contact model, Gauss integrations have to be performed over the surface of the body (in the reference configuration), i.e., a number of quadrilateral elements. Thus we are specifically interested in getting the surface unit out-normals ($\mathbf{N}$) at these Gauss integration points in the reference configuration. As shown in Fig. 15, we are interested in finding the unit out normal at the top surface of a generic hexahedron element located at $\mathbf{X} = (X_1, X_2, X_3)$ in the reference configuration. Consider the Jacobi matrix $\mathbf{J} = \frac{\partial \mathbf{X}}{\partial \boldsymbol{\xi}}$ that maps the element from the iso-parametric space to the corresponding physical domain. Denote $\boldsymbol{\xi} = (\xi, \eta, 1)$ as the corresponding point of interest in the iso-parametric space. It is easy to see that the unit surface out-normal at $\boldsymbol{\xi}$ is $\mathbf{N}_\xi = (0, 0, 1)$. Making use of the Nanson's formula $\mathbf{n}da = J\mathbf{F}^{-T}\mathbf{N}dA$ and by considering $\mathbf{J} = \frac{\partial \mathbf{X}}{\partial \boldsymbol{\xi}}$ as the corresponding deformation gradient of the two spaces, one can write

$$\mathbf{N}dA = \det(\mathbf{J})\mathbf{J}^{-T}\mathbf{N}_\xi dA_\xi \tag{84}$$

where dA and dA_ξ are the surface area elements.

Noticing that in the Eq. (84), dA, dA_ξ and $\det(\mathbf{J})$ are scalars and keeping in mind $\mathbf{N}$ is a unit vector, one may get

$$\mathbf{N} = \frac{\mathbf{J}^{-T}\mathbf{N}_\xi}{\sqrt{(\mathbf{N}_\xi\cdot\mathbf{J}^T\mathbf{J}\mathbf{N}_\xi)^{-1}}} \tag{85}$$

where $\mathbf{J}$ can be obtained through standard finite element method and $\mathbf{N}_\xi$ is always given once the corresponding surface is determined.

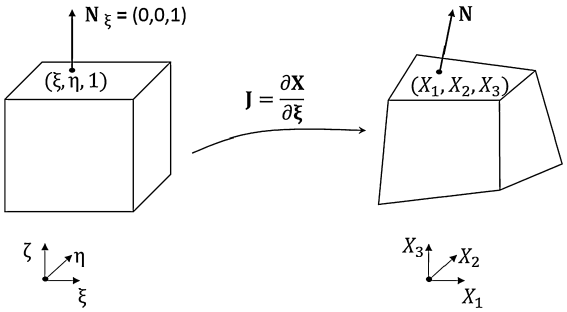

Fig. 15. A numerical way to obtain the initial surface unit out-normals.

References

[1] P. Wriggers, Computational Contact Mechanics, Springer, Hannover, 2003.
[2] T.A. Laursen, Computational Contact and Impact Mechanics: Fundamentals of Modeling Interfacial Phenomena in Nonlinear Finite Element Analysis, 1st edition, Springer, Berlin, 2002.
[3] Y.P. Zhao, X. Shi, W.J. Li, Effect of work of adhesion on nanoindentation, Rev. Adv. Mater. Sci. 5 (2003) 348–353.
[4] D. Saraev, R. Miller, Atomistic simulation of nanoindentation into copper multilayers, Model. Simul. Mater. Sci. Eng. 13 (7) (October 2005) 1089–1099.
[5] C.F. Sanz-Navarro, S.D. Kenny, R. Smith, Atomistic simulations of structural transformations of silicon surfaces under nanoindentation, Nanotechnology 15 (5) (May 2004) 692–697.
[6] G. Gao, C. Tahir, W.A. Goddard III, Energetics, structure, mechanical and vibrational properties of single-walled carbon nanotubes, Nanoscale 9 (1998) 184–191.
[7] T. Hertel, R. Walkup, P. Avouris, Deformation of carbon nanotubes by surface van der Waals forces, Phys. Rev. B 58 (20) (November 1998) 13870–13873.
[8] Y.P. Zhao, L.S. Wang, T.X. Yu, Mechanics of adhesion in MEMS—a review, J. Adhes. Sci. Technol. 17 (4) (January 2003) 519–546.
[9] G. Binnig, C.F. Quate, Atomic force microscope, Phys. Rev. Lett. 56 (9) (1986) 930–934.
[10] B. Cappella, G. Dietler, Force-distance curves by atomic force microscopy, Surf. Sci. Rep. 34 (1–3) (January 1999) 1–104.
[11] M. Lantz, S.J. O'Shea, M. Welland, Simultaneous force and conduction measurements in atomic force microscopy, Phys. Rev. B 56 (23) (December 1997) 15345–15352.
[12] T. Schlick, Molecular Modeling and Simulation: An Interdisciplinary Guide, Springer, New York, 2002.
[13] H. Minaki, S. Li, Multiscale modeling and simulation of dynamic wetting, Comput. Methods Appl. Mech. Eng. 273 (May 2014) 273–302.
[14] S. Li, H. Fan, On multiscale moving contact line theory, Proc. R. Soc. A 471 (2179) (2015) 20150224.
[15] J. Huang, X. Peng, C. Xiong, J. Fang, Influence of substrate stiffness on cell-substrate interfacial adhesion and spreading: a mechano-chemical coupling model, J. Colloid Interface Sci. 355 (2) (March 2011) 503–508.
[16] H. Fan, S. Li, Modeling microtubule cytoskeleton via an active liquid crystal elastomer model, Comput. Mater. Sci. 96 (January 2015) 559–566.
[17] K.L. Johnson, K. Kendall, A.D. Roberts, Surface energy and the contact of elastic solids, Proc. R. Soc. A, Math. Phys. Eng. Sci. 324 (1558) (September 1971) 301–313.
[18] B.V. Derjaguin, V.M. Muller, Yu.P. Toporov, Effect of contact deformations on the adhesion of particles, J. Colloid Interface Sci. 53 (2) (November 1975) 314–326.
[19] S. Cho, S. Park, Finite element modeling of adhesive contact using molecular potential, Tribol. Int. 37 (9) (September 2004) 763–769.
[20] M.P. Allen, D.J. Tildesley, Computer Simulation of Liquids, Oxford Science Publications, New York, 1989.
[21] D. Frenkel, B. Smit, Understanding Molecular Simulation: From Algorithms to Applications, 2nd edition, Academic Press, San Diego, 2001.
[22] A. Leach, Molecular Modelling: Principles and Applications, Pearson Education, 2001.
[23] G. Kloosterman, R.M.J.V. Damme, A.H. van den Boogaard, J. Huetink, A geometrical-based contact algorithm using a barrier method, Int. J. Numer. Methods Eng. 51 (February 2000) (2001) 865–882.
[24] R.A. Sauer, S. Li, A contact mechanics model for quasi-continua, Int. J. Numer. Methods Eng. 71 (January) (2007) 931–962.
[25] R.A. Sauer, S. Li, An atomic interaction-based continuum model for adhesive contact mechanics, Finite Elem. Anal. Des. 43 (5) (March 2007) 384–396.
[26] J.N. Israelachvili, Intermolecular and Surface Forces, 3rd edition, Academic Press, 2011.
[27] K. Bathe, Finite Element Procedures, Prentice-Hall, Englewood Cliffs, NJ, 1996.
[28] T.J. Hughes, The Finite Element Method: Linear Static and Dynamic Finite Element Analysis, Courier Dover Publications, 2012.
[29] C. Argento, A. Jagota, Surface formulation for molecular interactions of macroscopic bodies, J. Mech. Phys. Solids 45 (7) (1997).
[30] A. Jagota, C. Argento, An intersurface stress tensor, J. Colloid Interface Sci. 191 (2) (July 1997) 326–336.
[31] T. Belytschko, W. Kam Liu, B. Moran, Nonlinear Finite Elements for Continua and Structures, Wiley, Chichester, 2000.
[32] G.A. Holzapfel, Nonlinear Solid Mechanics, Wiley, Chichester, 2000.
[33] F. Armero, E. Petocz, Formulation and analysis of conserving dynamic contact/impact algorithms problems for frictionless, Comput. Methods Appl. Mech. Eng. 158 (1998) 269–300.